Design and performance of feedhorn-coupled bolometer arrays for SPIRE

Brooks Rownd, James J. Bock, Goutam Chattopadhyay, Jason Glenn, Matthew J. Griffin

Brooks Rownd, James J. Bock, Goutam Chattopadhyay, Jason Glenn, Matthew J. Griffin, "Design and performance of feedhorn-coupled bolometer arrays for SPIRE," Proc. SPIE 4855, Millimeter and Submillimeter Detectors for Astronomy, (17 February 2003); doi: 10.1117/12.459372

SPIE.

Event: Astronomical Telescopes and Instrumentation, 2002, Waikoloa, Hawai'i, United States

Design and performance of feedhorn-coupled bolometer arrays for SPIRE

B. Rownd[a], J.J. Bock[b], G. Chattopadhyay[c], J. Glenn[a], and M. Griffin[d]

[a]CASA-ARL, Univ. of Colorado, 1255 38th Street, Boulder, CO 80303
[b]Jet Propulsion Laboratory, MS 169-327, 4800 Oak Grove Drive, Pasadena, CA 91109
[c]Dept. of Physics, MS 59-33, Caltech, Pasadena, CA 91125
[d]Physics and Astronomy Dept., Cardiff University, Wales, UK

ABSTRACT

This paper reviews the design, modeling, and testing of feedhorn arrays coupled to bolometric detector arrays being developed for the ESA Herschel Space Observatory's SPIRE instrument. SPIRE will incorporate five arrays of silicon nitride micromesh bolometers, in three broadband photometers and two Fourier-Transform spectrometers covering 200-700 μm, with a total of 326 feedhorn-coupled bolometers. The precision feedhorn arrays are formed by close-packing individually fabricated conical feedhorns, which terminate in waveguides and integrating cavities. The detector array is efficiently packaged by mounting it between a metallized silicon backshort array and the feedhorn array, which encloses the bolometers in precisely tuned integrating cavities. The absorption efficiency, bandwidth, and cross talk were first investigated with numerical simulations of the electromagnetic fields, and then measured for prototype arrays in a test facility. This discussion describes the design goals, simulations, fabrication, and measurements of optical efficiencies, spectral properties, beam shapes, and cross talk between bolometers.

Keywords: feedhorns, bolometers, SPIRE, Herschel Space Observatory, submillimeter

1. INTRODUCTION

The Herschel Space Observatory is an ESA "cornerstone" mission, scheduled for launch in 2007, which will study the Universe at sub-millimeter wavelengths (60 μm - 700 μm) that are not easily accessible to ground-based instrumentation. Submillimeter wavelengths are particularly important for the study of star formation activity within galaxies, where much of the luminosity from hot young stars is radiated in the far-infrared (FIR) and submillimeter by interstellar dust grains, and for deep observations tracing the star formation history of the Universe. Within our own galaxy, sub-millimeter wavelength observations with Herschel's sensitive large-format arrays will allow detailed study of star formation activity by penetrating the dusty, opaque star-forming environments.

SPIRE (the Spectral and Photometric Imaging REceiver) is one of three science instruments on board the Herschel Space Observatory. The others are PACS[1] and HIFI.[2] SPIRE[3] is composed of two complimentary instruments, a three-band imaging photometer and an imaging Fourier Transform Spectrometer (FTS), each covering the 200 μm - 700 μm band. Both instruments are based on the same Si_3N_4 micromesh bolometer technology[4] that has been proven in ground-based and sub-orbital millimeter-wavelength instrumentation, and is being implemented both here and elsewhere for space-based experiments. SPIRE's multifrequency photometer instrument consists of three simultaneously-imaging bolometer arrays with 43, 88 and 149 bolometers, in bands centered at 500 μm, 350 μm and 250 μm respectively. The FTS instrument has two simultaneously-imaging focal planes of 19 and 37 bolometers, covering 200 μm - 315 μm and 315 μm - 670 μm respectively, that together allow efficient coverage of the wide frequency coverage of the instrument.

Further author information: (Send correspondence to J.G.)
B.K.R.: e-mail: brooks.rownd@casa.colorado.edu
J.G.: e-mail: jason.glenn@casa.colorado.edu

Millimeter and Submillimeter Detectors for Astronomy, Thomas G. Phillips, Jonas Zmuidzinas, Editors, Proceedings of SPIE Vol. 4855 (2003) © 2003 SPIE · 0277-786X/03/$15.00

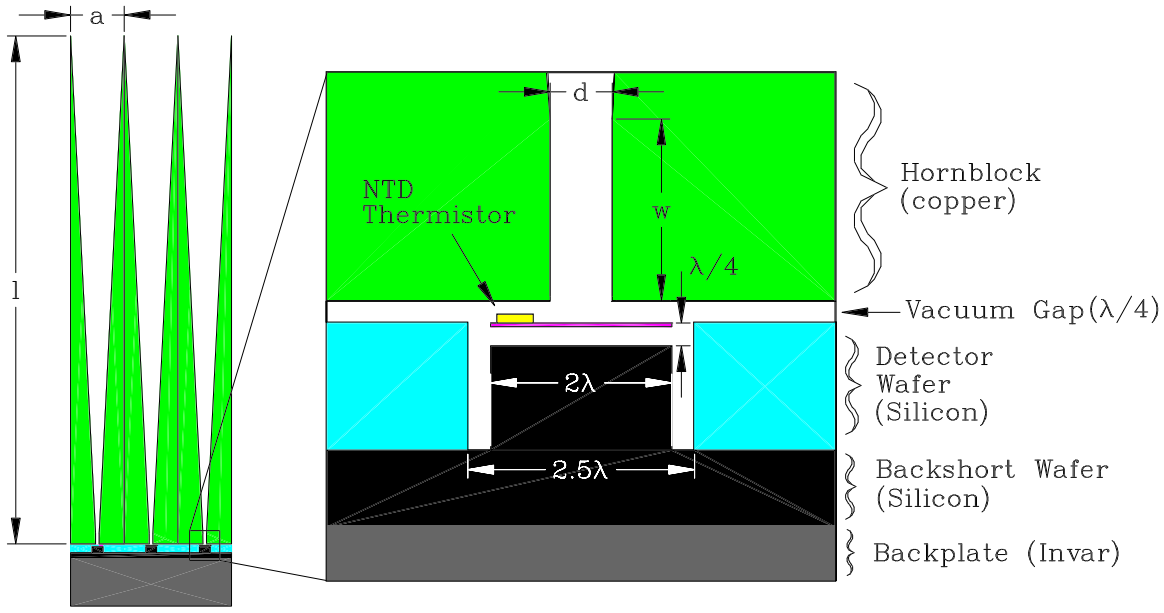

Figure 1. This is a cross-section of A SPIRE detector array, showing the relative sizes of the feedhorn, waveguide section and the detector cavity. The dimensions labelled on the figure are listed for each SPIRE array in Table 1.

The development of large feedhorn-coupled submillimeter wavelength bolometer arrays has been greatly simplified by recent advances in micromesh bolometer fabrication, which enable high yield micromesh detector arrays on individual silicon wafers. The monolithic design allows efficiently packaging of these arrays in a simple fixture, sandwiched between a backshort plate and the precision feedhorn block. This technique has been successfully implemented in the Bolocam instrument.[5,6] The importance of this work is that the SPIRE program depends on the production of large numbers of precise feedhorns with 5 μm tolerances that are efficiently coupled to large bolometer arrays. The success of the technique for constructing these arrays is evaluated by measurement of the beam shapes, spectroscopy and optical efficiencies, and through the comparison of these measurements to both the theory behind the design and numerical simulations.

2. DESIGN & FABRICATION

The basic construction of the SPIRE detector arrays is shown in Figure 1. The construction and properties of similar micromesh bolometer arrays have been presented by Turner et al.,[7] so the detector wafer will not be discussed in detail here. The detector wafer is mounted on a second metallized wafer that has been etched to form tuned backshorts, and both are fixed to an invar backplate which minimizes mechanical stress on the silicon during thermal cycling, and keeps the detectors aligned. The feedhorn block is mounted on the invar backplate so that it is suspended over the detector wafer and maintains a safe vacuum gap between them. The back of the feedhorn block will also be referred to as the "frontshort". As described later in this paper, the lack of a sealed integrating cavity does not cause substantial loss or cross talk among the detectors. The feedhorn array is designed with a spacing of nearly $2f\lambda$ for the $f/5$ feeds, and each feedhorn is coupled to its detector cavity by a section of circular waveguide. For convenience, the five SPIRE detector arrays have been designated "P/SW", "P/MW", and "P/LW" for the short, medium and long wavelength photometers, and "S/SW" and "S/LW" for the short and long wavelength spectrometers, respectively. For each array, the dimensions indicated in Figure 1 are listed in Table 1.

The feedhorns are a simple conical design, for which the main design consideration was efficient coupling to the incoming radiation, while mimizing the manufacturing cost of the feedhorn block. Sidelobes were not a major concern, because the SPIRE optical system uses a cold Lyot stop at an image of the primary mirror.

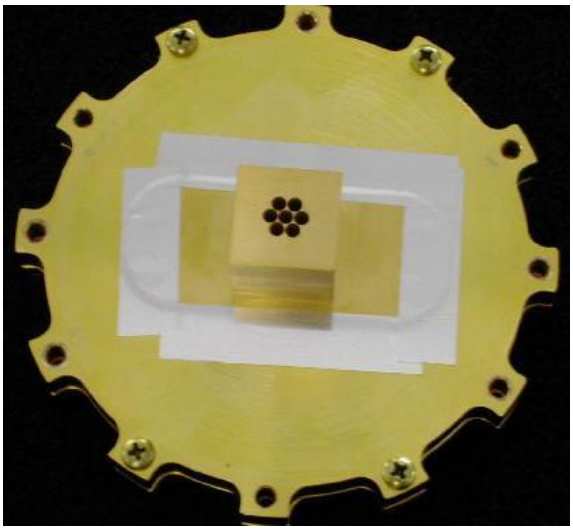

Figure 2. A photograph of the short-wavelength photometer (P/SW) prototype feedhorn array.

This design eliminates the need for expensive corrugations in the feedhorns. The diameter of the short section of circular waveguide was tuned to conveniently provide sharp high-pass filtering at the edge of the intended bandpass. The integrating cavities have a diameter of $2.5\lambda_c$, centered on the $2\lambda_c$ diameter micromesh absorber which was located $\lambda_c/4$ from both the frontshort and backshort. Numerical simulations, described in Section 3, were used to guide the carefully tuned design of the integrating cavities for each feedhorn array, and to check the effect of manufacturing tolerances on the absorption efficiency of the detector.

Table 1. Feedhorn Dimensions

Array	λ_c (μm)	Length, l (mm)	Aperture, a (mm)	Waveguide Dia., d (μm)	Waveguide Length, w (μm)
P/SW	250	23.68	2.40	171	500
P/MW	350	32.75	3.23	246	700
P/LW	500	46.36	4.90	353	1000
S/SW	275	23.68	2.15	190	550
S/LW	450	46.36	3.80	395	900

Custom Microwave Inc.[8] of Longmont, CO manufactured the prototype feedhorn blocks, using the same technique as for the full-scale qualification models. Individual feedhorns were formed by machining a negative image of the feedhorn's interior and waveguide on aluminum mandrels, gold plating these and then electroforming copper onto them. The electroformed mandrels were turned down to cylindrical feedhorn inserts, then aligned and soldered into the feedhorn blocks. The aluminum mandrels were then etched away, leaving the finished feedhorn block. Figure 2 shows the completed prototype P/SW array mounted in the test fixture.

3. BOLOMETER CAVITY SIMULATIONS

High Frequency Structure Simulator (HFSS)[9] software was used to simulate the propagation and absorbtion of electromagnetic fields in models of the waveguide and detector cavities, allowing optimization of the designs to acheive maximium optical efficiency. Detailed descriptions of similar simulations have been published by Glenn

et al.[10] and Chattopadhyay et al.,[11] showing that it is possible to accurately predict how changes in the cavity and absorber dimensions affect optical efficiencies. In all but one case, the simulations are single-moded and monochromatic.

The first result of these simulations was a simple comparison of both single-mode and multi-mode optical efficiencies for the P/SW model. A multi-mode model was created by opening the waveguide diameter from 171 μm to 278 μm to admit the TM_{01} and TE_{21} modes. As the data in Table 2 indicate, the primary TE_{11} mode couples better than the higher order modes. The multi-mode simulations were conducted by first modelling each mode individually, and then all three modes simultaneously. Due to interactions among the fields and with the absorber, the efficiency derived from the simultaneous modelling of all three modes is not equivalent to a simple linear combination of the efficiencies derived for them individually. The multi-mode results are important for understanding the relative absorption of the different modes in SPIRE's two wide band spectrometer arrays, and for the measurement of S/LW optical efficiencies in the lab.

Table 2. Simulation Results

Array	λ_{sim} μm	Waveguide Dia. (μm)	Mode	Absorbtion Efficiency
P/SW	250	171	TE_{11}	85%
P/SW	250	278	TE_{11}	97%
P/SW	250	278	TM_{01}	56%
P/SW	250	278	TE_{21}	78%
P/SW	250	278	TE_{11}+TM_{01}+TE_{21}	72%
S/SW	225	190	TE_{11}	93%
S/SW	250	190	TE_{11}	92%
S/SW	275	190	TE_{11}	80%
S/LW	349	410	TE_{11}	97%
S/LW	448	410	TE_{11}	90%
S/LW	667	410	TE_{11}	50%

It was anticipated that additional mechanical clearance between the feedhorn block and the delicate detector wafer might be necessary in some situations, increasing the vacuum gap and frontshort distance. Numerous simulations were conducted to test whether displacement of the frontshort or backshort distances from the nominal $\lambda_c/4$ value would either substantially change the optical efficiency, or widen the response at the edges of the band. To this end, the next set of simulations measured the optical efficiency of the P/SW model at 250 μm, with the frontshort displaced from 0 to 50 μm above its nominal $\lambda_c/4$ distance from the absorber. The optical efficiency of the cavity was found to increase to 88% at a frontshort displacement of 25 μm, and then fall back to the nominal value of 85% for a 50 μm displacement. This shows that the optical efficiency of the detector is quite tolerant to such displacements in the frontshort distance. Simulations of the wide bandwidth spectrometer models also show that frontshort displacements of up to 50 μm produce only a few percent change in optical efficiency. Additional simulations were conducted to evaluate the frequency dependence of the absorption efficiency near the waveguide cutoff frequency. Again, small displacements in either the frontshort or backshort distances produced only small changes in the absorbtion as a function of frequency near the waveguide cutoff, which is tightly controlled by the diameter of the waveguide.

Finally, simulations were conducted to model the level of cross talk between adjacent detectors. Since the sides of the integrating cavities are not metallized, it is possible for power to be diffracted or scattered laterally through either the vacuum gap or silicon to adjacent detectors. These simulations find that less than 0.5% of the power leaking out of any cavity is absorbed in any adjacent detector.

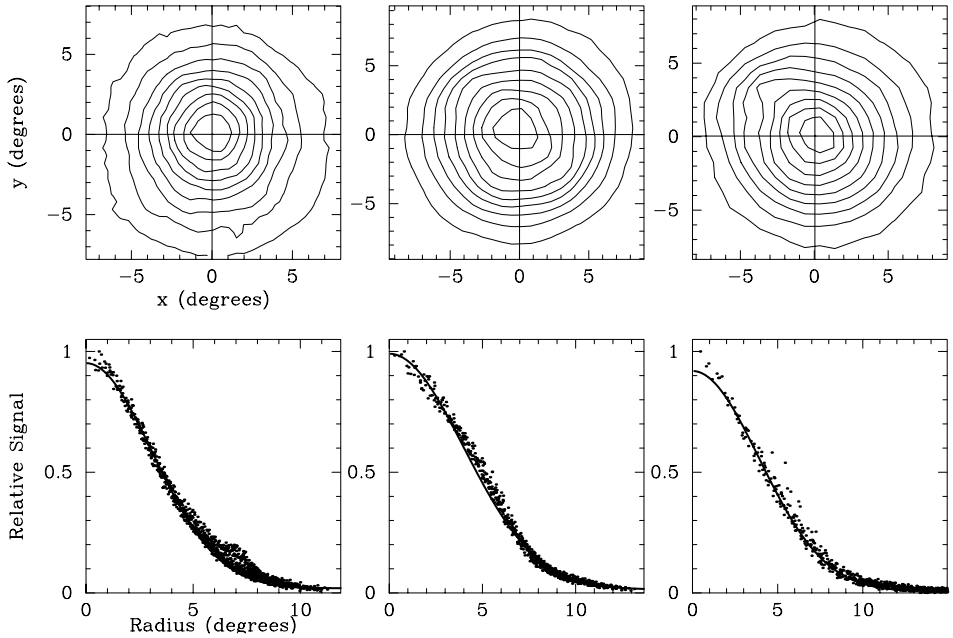

Figure 3. The upper panels show representative beam maps for all three tested bandpasses. Each map has a different scaling and resolution. Left to right they are the 250 μm P/SW, and the 350 μm and 450 μm S/LW arrays. The spatial axes are measured in degrees from the beam centroids, and the contours are spaced at every 10% of the peak value. The lower panels plot the data radially from the centroid, with a Gaussian fit to the data plotted on top for reference. The spur in the upper left of the 450 μm map is caused by a filter defect.

4. TESTING PROGRAM

The prototype feedhorn arrays were tested in the Submillimeter Astrophysics Lab at the University of Colorado, Boulder. Only two arrays, the P/SW and the S/LW, were chosen for testing as prototypes. The short-wavelength photometer array was chosen because it has the tightest manufacturing tolerances, which allows a determination of whether the manufacturing process is producing horns with the expected optical properties. The long-wavelength spectrometer array was chosen because it operates over the widest frequency range, over which it is desirable to determine the behavior of the beam shapes and optical efficiencies. Three detectors were tested in each array, and the P/SW was tested with a 250 μm bandpass while the S/LW was tested with both 350 μm and 450 μm bandpasses.

The prototype arrays were installed in a liquid helium cryostat, with a closed-cycle ^{3}He cryocooler to cool the focal plane to the 300 mK operational temperature of the detectors. The array observes external sources through a filter stack consisting of a bandpass filter, a 0.9%-transmission neutral density filter (NDF), a stack of 3 or 4 non-parallel low-pass filters, and finally a thin room-temperature HDPE dewar window. These filters are not intended to match the actual SPIRE filter stack. The filters are installed on the radiation shields, with indium gaskets to ensure light-tight interfaces and good thermal contact. The bolometers are configured in a balanced circuit and share a common bias distributed through a load resistor array. The signal lines are buffered from external noise sources by low noise source-follower JFET amplifiers located in a shielded box nearby in the 4K space. A shielded preamplifier box mounted on the outside of the dewar completes the amplifier chain.

4.1. Beam Mapping

The beams were mapped by observing a temperature-controlled blackbody source mounted on a linear two-axis stepper-motor track, which was controlled by the data acquisition computer. The blackbody source was heated to 900^{o}C, and chopped at the adjustable aperture by a frequency-stabilized chopper blade. A lock-in amplifier demodulated the chopped bolometer signal, and smoothed it with a 100 ms time constant prior to being sampled by the data aquisition computer. The blackbody source was stepped through a uniformly incremented square

grid of positions, allowing three seconds for the blackbody source and detector signal to settle before sampling the detector signal and moving on to the next grid position.

Table 3. Beam Sizes

Array/Band	Modes	Calculated TE_{11} HPBW	HPBW
P/SW 250 μm	TE_{11}	7.0^o	$7.2^o \pm 0.3^o$
S/LW 350 μm	TE_{11},TM_{01},TE_{21}	5.9^o	$9.9^o \pm 0.2^o$
S/LW 450 μm	TE_{11},TM_{01}	7.3^o	$8.4^o \pm 0.3^o$

Figure 3 shows a beam map and its radial profile for each of the three tested bandpasses. Each beam is fit with a Gaussian model to determine its FWHM, and the resulting fit is plotted over the data showing that the beams are consistent with a Gaussian form. The beam sizes derived from these fits are listed in Table 3, along with the expected HPBW calculated from the band-center frequency and feedhorn aperture for the TE_{11} mode alone. The single-mode 250 μm beam size is consistent with the expected TE_{11} mode diffraction limit, whereas the multi-mode 350 μm and 450 μm beams are 68% and 15% larger, respectively. This is evidence that the S/LW beams include contributions from the TM_{01} and TE_{21} modes, which are not centrally peaked. The observed beam sizes can be understood by considering the different impedance mismatches for each mode at the transition between the waveguide section and the detector cavity, and at the absorber itself. The feedhorn and detector designs were optimized to efficiently propagate the TE_{11} mode and couple it to the absorber, whereas the design is not tuned to higher order modes, and that they are not expected to couple as well. The fact that the 450 μm beam does not show much broadening over the beam size expected for the TE_{11} mode alone indicates that the TM_{01} mode couples poorly to the detector for the 450 μm bandpass, which is consistent with the low absorbtion efficiency for this mode found by the simulations. The optical efficiencies presented in Section 4.3 are consistent with the expectation of a low absorbtion efficiency for the TM_{01} mode in the 450 μm S/LW array. In contrast, the 350 μm S/LW beam shows substantial broadening from the higher order modes, indicating that they are absorbed reasonably well. A more detailed analysis of the coupling of each mode to the detector, and the resulting beam shapes is in progress.

4.2. Spectroscopy

The spectral responses of the detector and feedhorn arrays were measured for each bandpass, in combination with the filter stack, using a Bruker IFS-120HR far-infrared Fourier transform spectrometer.[12] The experiment was positioned to observe fringes from the spectrometer at the side exit port, with an HDPE lens to couple the beam to the focal plane. A representative transmission spectrum for each test band is depicted in Figure 4, along with the expected bandpass for each filter stack as derived by multiplying through the transmission spectra of the individual filters.

Table 4. Bandpass Properties

Array	Band	ν_o (GHz)	$\Delta\nu$ (GHz)
P/SW	250	1212	263
S/LW	350	844	98
S/LW	450	657	124

The measured transmission spectra are consistent with the expected positions and widths of each bandpass, and their properties tabulated in Table 4. The spectroscopy also shows that standing waves are present in

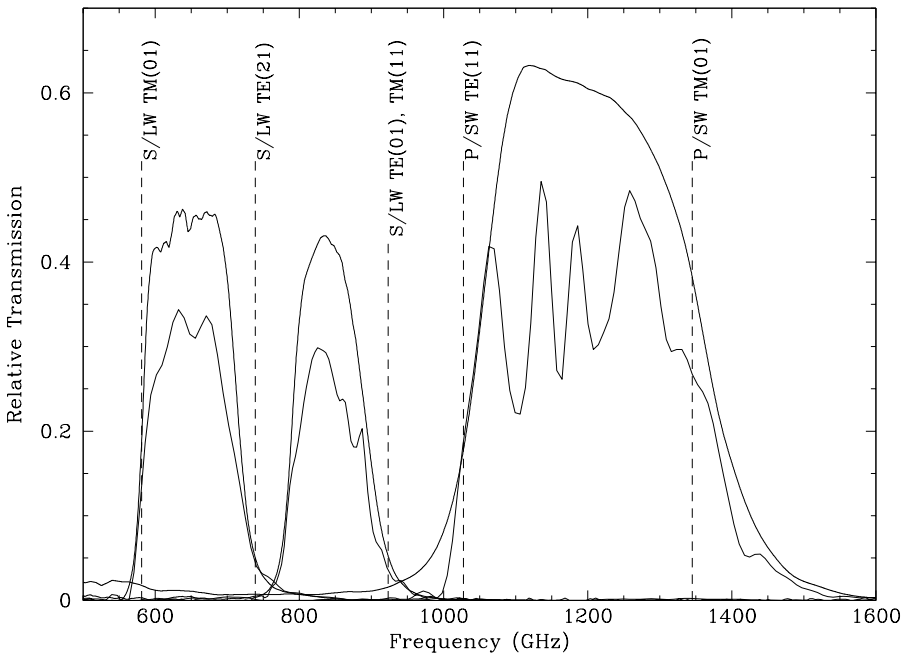

Figure 4. The expected (upper) and measured (lower) bandpass transmission profiles are plotted together here, along with indications of cutoff frequency of the waveguide for each mode in both the P/SW and S/LW arrays. The expected bandpasses are the product, through the filter stack, of each filter's individually measured transmission spectrum. The lower curves are the actual response measured in the lab, which shows some fringing due to standing waves between the filters.

some of the channels, though an effort was made to prevent this by tilting the filters at various angles so that consecutive filters in the stack are not parallel. The strengths of these resonances vary somewhat for adjacent horns. The redundant low-pass filters in each filter stack should prevent any high frequency leaks, whereas the waveguide section of each feedhorn naturally provides sharp high-pass filtering. The cutoff frequencies of several relevant modes for each feedhorn block are shown in Figure 4. Since the bandpasses are designed to avoid these cutoffs, they are not seen in this spectroscopy, however further testing without the bandpass filters is underway to measure these cutoff frequencies.

4.3. Optical Efficiencies

The optical efficiencies of the detectors were derived by comparing $I-V$ load curves measured under optical loading from blackbody sources of various temperatures which completely filled the beams. Measurements were made of blackbody sources external to the dewar, as well as and an internal temperature-controlled "cold calibrator" blackbody source. The cold calibrator consists of a thermally isolated, grooved slug of Eccosorb,[13] which is heated by applying current to an embedded resistor, and whose temperature is monitored with a calibrated germanium 4-wire thermometer. The external loads consist of Eccosorb foam, observed both at room temperature and immersed in a 77 K liquid nitrogen bath. The calculations include a correction for 5% reflection off of the surface of the liquid nitrogen onto room temperature surfaces.

Figure 5 shows a representative load curve for each bandpass, obtained while viewing external hot and cold loads. The absorbed optical power is derived as shown, by measuring the offset in electrical bias power dissipated in the detector along lines of constant bolometer resistance. The hot and cold loads are measured in a cold/hot/hot/cold rotation so that any linear heating effect on the focal plane and filters can be detected, and removed by averaging the data. The power offset between the resistance vs. bias power curves, from which the

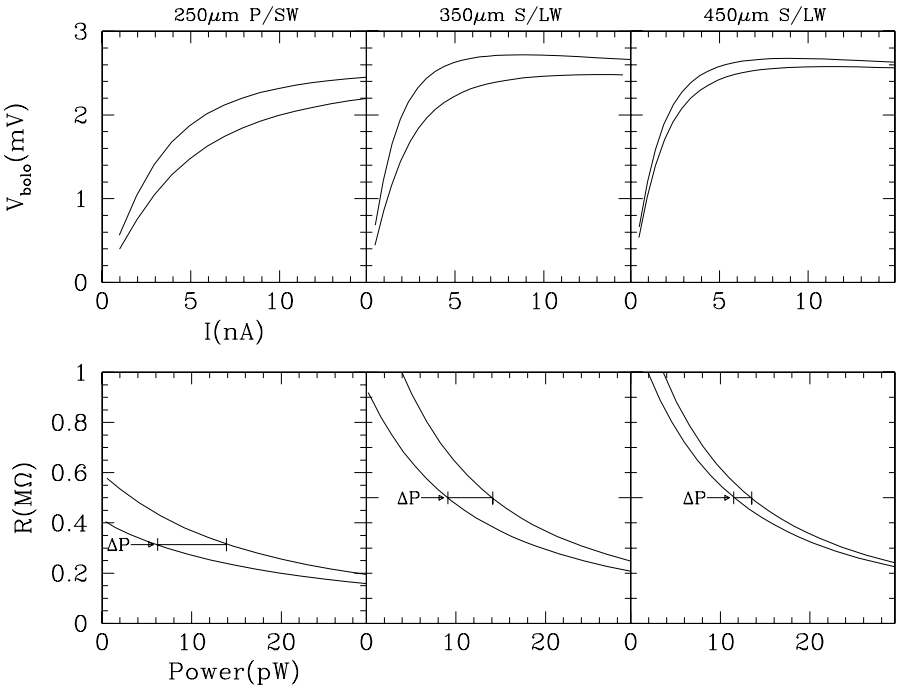

Figure 5. Representative load curves are presented for the three test bandpasses. The top row of plots shows the measured load curves (voltage vs. current at the bolometer) measured while observing Eccosorb foam at both room temperature and immersed in a liquid nitogen bath. In the bottom row the bolometer resistance is plotted against the electrical bias power dissipated in the bolometer. The difference in absorbed optical power between the two loads is simply the shift between the two curves along lines of constant resistance, and is measured as depicted.

optical efficiency is derived, is larger at lower bolometer resistances. This could be due to local heating of the array at increased power levels, artificially lowering the bolometer resistances at higher loading, and increasing the calculated optical efficiencies. If this is true, then the optical efficiencies measured with the cold calibrator source could be lower than those measured from "hot" sources outside the dewar.

Table 5. Optical Efficiencies

Array	Band (μm)	ΔP(calc.) (pW)	ΔP(meas.) (pW)	optical efficiency
P/SW	250	10.7	8.6±0.5	80±5%
S/LW	350	7.2	4.9±0.2	68±3%
S/LW	450	3.8	2.1±0.2	56±5%

Optical efficiencies derived from the load curves are listed in Table 5. The listed uncertainties are statistical, and do not represent systematic effects. The (mostly) single-mode 250 μm P/SW band has an optical efficiency of $80\% \pm 5\%$, which is in good agreement with the expectation of 85% found at the center of the band in the simulations. The S/LW results are more complex due to the multi-mode nature of the bands. For the 350 μm band an optical efficiency of $68\% \pm 3\%$ is derived, assuming that the three expected modes are present in this bandpass. This specific feedhorn and cavity was not numerically simulated, but a comparison with the 3-mode

simulation made for the P/SW model should be informative. The 3-mode P/SW simulation yielded an optical efficiency of 72%, in good agreement with the 350 μm S/LW measurement. The 450 μm S/LW band has only two modes, and it yielded a somewhat lower optical efficiency of $56\% \pm 5\%$. This is evidence that the second mode (TM_{01}) does not couple well for this bandpass, which is in agreement with the observation that the 450 μm S/LW beam size shows very little broadening from this mode.

Cold calibrator load curves were measured for the 250 μm band. An optical efficiency of $67\% \pm 7\%$ was derived from this cold calibrator measurement, which is somewhat lower than that derived from observing external loads. A similar 350 μm micromesh bolometer experiment documented by Turner et al.[7] also measured somewhat lower cold calibrator optical efficiency. This indicates that systematic uncertainties in the optical efficiency measurements might be as high as 10%.

Simulations of cross talk between detectors show less than 1% cross talk between adjacent bolometers. Crosstalk measurements were made with the 250 μm P/SW array by blocking all but one of the feedhorn apertures in the array, and measuring the response to a chopped external blackbody signal on all bolometers with a lock-in amplifier. For the "dark" detector adjacent to the unobstructed feedhorn, cross talk was measured at 0.45% of the unobstructed detector's signal, with a signal-to-noise ratio of 3. At the detector two pixels from the unobstructed feedhorn, cross talk was measured to be 0.15%, with a signal-to-noise ratio of just less than 2. This demonstrates that cross talk is indeed low, consistent with the simulation results.

5. CONCLUSION

This paper has described the design, simulation, fabrication and testing of prototype arrays of feedhorn-coupled bolometers for the SPIRE instrument on the Herschel Space Observatory. The results presented in this paper confirm that the SPIRE detector arrays have achieved high optical efficiencies with tight fabrication tolerances, and that their performance was consistent with the results of numerical modelling. The beam patterns and spectral responses were found to be consistent with the expectations of the design theory. Further testing and simulations are in progress to observe the waveguide cutoff frequencies, improve the systematics in the optical efficiency measurements, and model the theoretical beam patterns for few-moded feedhorns.

ACKNOWLEDGMENTS

We would like to gratefully acknowledge Martin Caldwell, Anthony Murphy and Clency Lee-Yow for useful discussions related to feedhorn design.

REFERENCES

1. C. A. Poglitsch, Waelkens, and N. Geis, "The Photodetector Array Camera and Spectrometer (PACS) for Herschel," in *The Promise of the Herschel Space Observatory*, G. Pilbratt, J. Cernicharo, A. Heras, T. Prusti, and R. Harris, eds., pp. 29–36, symposium held 12-15 December 2000, Toledo, Spain, ESA SP-460, July 2001.
2. T. de Graauw and F. Helmich, "Herschel-HIFI: The heterodyne instrument for the far-infrared," in *The Promise of the Herschel Space Observatory*, G. Pilbratt, J. Cernicharo, A. Heras, T. Prusti, and R. Harris, eds., pp. 45–51, symposium held 12-15 December 2000, Toledo, Spain. ESA SP-460, July 2001.
3. M. Griffin, L. Vigroux, and B. Swinyard, "SPIRE: a bolometer instrument for first," in *Advanced Technology MMW, Radio, and Terahertz Telescopes*, T. Phillips, ed., *Proc. SPIE* **3357**, pp. 404–413, 1998.
4. P. Mauskopf, J. Bock, H. D. Castillo, W. Holzapfel, and A. Lange, "Composite infrared bolometers with Si_3N_4 micromesh absorbers," *Appl. Opt.* **36**, pp. 765–771, 1996.
5. J. Glenn, J. Bock, G. Chattopadhyay, S. Edgington, A. Lange, J. Zmuidzinas, P. Mauskopf, B. Rownd, and L. Yuen, "Bolocam: a millimeter-wave bolometric camera," in *Advanced Technology MMW, Radio, and Terahertz Telescopes*, T. Phillips, ed., *Proc. SPIE* **3357**, pp. 326–334, 1998.
6. e. a. J. Glenn, "Current status of bolocam: a large-format millimeter-wave camera," these proceedings, 2002.

7. A. Turner, J. Bock, J. Beeman, J. Glenn, P. Hargrave, V. Hristov, H. Nguyen, F. Rahman, S. Sethuraman, and A. Woodcraft, "Silicon nitride micromesh bolometer array for submillimeter astrophysics," *Appl. Opt.* **40**, pp. 4921–4932, 2001.
8. Custom Microwave Inc., Longmont, CO. 80501.
9. High-Frequency Structure Simulator (HFSS), Ansoft Corporation, Four Station Square, Suite 200, Pittsburgh, PA. 15219.
10. J. Glenn, G. Chattopadhyay, S. Edgington, A. Lange, J. Bock, P. Mauskopf, and A. Lee, "Numerical optimization of integrating cavities for diffraction-limited millimeter-wave bolometer arrays," *Appl. Opt.* **41**, pp. 136–142, 2002.
11. G. Chattopadhyay et al., in preparation.
12. Bruker Optics Inc., Billerica, MA. 01821.
13. Emerson and Cumming Microwave Products, Inc., Woburn, MA. 01888.